Noel Howley - nh693

August 2022

1 Introduction

The use of proton beam radiotherapy has been a topic of growing interest, with key dependence relying on the use of Spread Out Bragg Peaks, SOBP's, to target a desired tumor region. SOBP's can be interpreted as the cumulative collection of multiple individual Bragg Curves, otherwise known as the Depth-Dose distribution curves, which are at the heart of the problems we are to work towards addressing in this documentation. In practice, depending on the target region required and the target dosage required, the initial energy of the proton beams vary in order to change properties of the Bragg curve, and hence the associated SOBP. Intensity of a Bragg curve can be interpreted as multiplying the equation of the Bragg curve by a constant. It is important to note that unless specified otherwise all plots will have standard intensity of unit value.

In this paper we shall be showcasing 4 different models of Bragg curves and hence SOBP's, all with unique qualities and differences. This PDF works in conjunction with the associated Jupyter notebook, of which contains all the relevant information necessary to retrieve the plots and data in the forthcoming documentation. The first of which is the what shall be named "Bortfeld's General Model" (Bortfeld, 1997), Many dose-depth plots in this documentation are plotting dose per fluence along the y-axis. This is equivalent to plotting "total absorbed dose" by the medium our beam is travelling through, the units for this unit of measure is $Gycm^2 \cdot 1.602 \cdot 10^{-10}$.

2 Model 1. Bortfeld's General Model

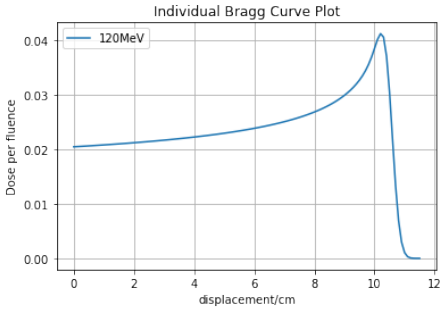

Figure 1: BGM: Bragg Curve of Initial Energy, $E_0 = 120\text{MeV}$

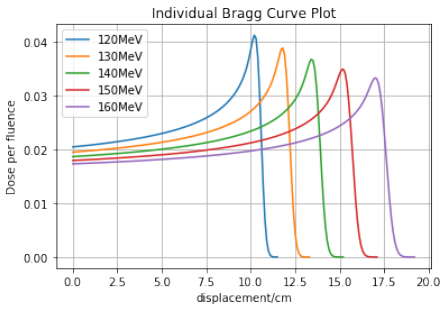

Figure 2: BGM: Bragg Curves with varying Initial Energy

As previously mentioned, the first model to be examined is the analytical model proposed by Bortfeld [1] and provides the necessary "starting point" for further examination.

2.1 Predefined Assumptions: Model 1. Bortfeld's General Case Model

- Density of whole medium is assumed to be equivalent of the density of water, many parameters are calculated with this in mind too as we shall mention more later.
  $\rho = 997kg/m^3$.

- An individual Bragg Curve takes the Equation:

$$D(x, E_0) = \Phi_0 \frac{e^{-\zeta^2/4}\sigma^{1/p}\Gamma(1/p)}{\sqrt{2\pi}\varrho p\alpha^{1/p}(1+\beta R_0)}[\frac{1}{\sigma}\mathbb{D}^{-\zeta}_{-1/p} + (\frac{\beta}{p} + \frac{\gamma}{\beta} + \frac{\epsilon}{/}R_0\mathbb{D}_{-1/p-1}(-\zeta))] \tag{1}$$

  Where $\mathbb{D}$ is the Parabolic Cylinder Function (Weisstein, 2002),

$$\Phi_0 = 1 + \beta R_0 \tag{2}$$

$$\zeta = \frac{R_0 - x}{\sigma} \tag{3}$$

  Further details on the variables used in the model can be found in (Bortfeld, 1997), of which many depend on the Initial Energy, E_0.

2.2 Behaviors of Bragg Curves

Using the model as defined above, we can see that different E_0 values contribute to different displacement of the peak dose value and of the Bragg curve. Furthermore, the value of the peak dose changes with different E_0 values.

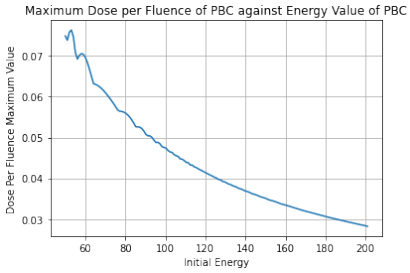

Figure 3: D_{peak} against Initial Energy

Before claiming correlations we should define terms.

Let, $y = D(x)$ represent (1) of the Dose-Depth Bragg curve. Hence, we may let the position of the peak be denoted x_{peak}.

$$x_{peak} := \mathrm{argmax}(y). \tag{4}$$

We may also define the Dose value of the x_{peak} as

$$D_{peak} = y(x_{peak}) \tag{5}$$

It is clear to see from figure 2 that there exists some relation between initial energy, E_0, and peak dose made clear by reviewing Figure 3. Therefore, when reference is made to alter the displacement of the peak dose, either altering E_0 or x_{peak}, with respect to the required units, shall achieve the same outcome.

2.3 BGM: Behaviours of SOBP's

From figure 2 we have established that there are unique properties to each unique values of E_0. We should benefit from reviewing the cumulative curve of n individual Bragg Peaks if we are in hope of solving an issue with a cumulative collection of Bragg peaks. Figure 4 shows a plot of a simple SOBP plot from our model.

2.3.1 Uncertainty

Should there be some error in our medium density, we can model the outcome of our Bragg peak and SOBP with the ranges of outcomes in the forms of a Monte Carlo approach and Error Bars.

We can approximate the uncertainty of a projection of a Bragg curve through other mediums by manipulating the model $f(z)$ to $f(z + \phi)$ where we let ϕ is

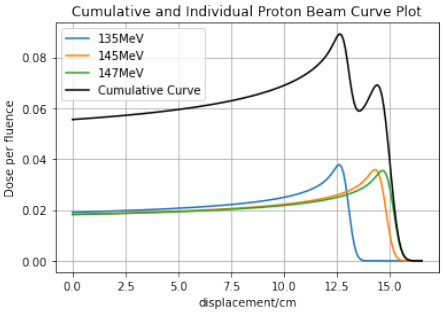

Figure 4: BGM: SOBP Behaviours

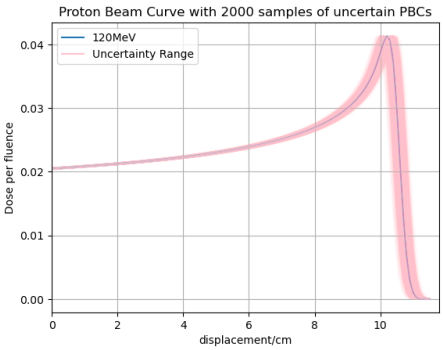

Figure 5: Monte Carlo approach to show Uncertainty Range for some ϕ

some Error value, s.t. $\phi \sim N(0, \theta)$ for some small θ. Note θ is the standard deviation not the variance. The ratio of $z : \phi$ will relate to the ratio between the control density, ρ_c, and the wanted approximation density, ρ_{aprox}.
Hence,

$$z : \phi = \rho_c : \rho_{\text{aprox}}. \tag{6}$$

Therefore, percentage error can be calculated.

A Monte Carlo approach can be seen in Figure 5 which represents the given uncertainty for some small ρ_{aprox}.

As we know the nature by which ϕ is distributed, we can therefore calculate the probability that a certain curve may be displaced by some amount. This nicely leads us onto the topic of accuracy.

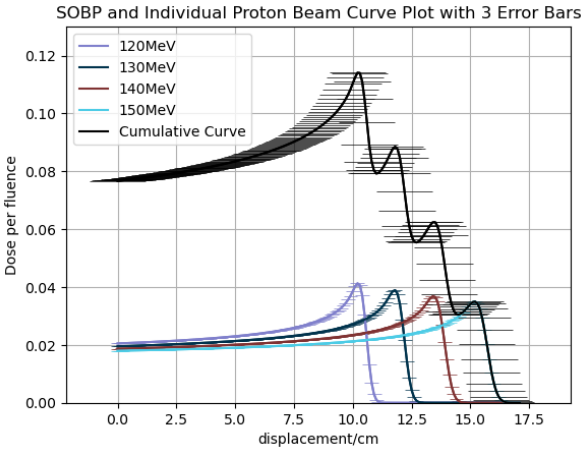

Figure 6: Error Bars for given ϕshown over Bragg curves and SOBP

2.3.2 Accuracy

The accuracy of which we require can be calculated subsequently from knowing the distribution of ϕ. As $\phi \sim N(0, \theta)$ we recall the values of which the total percentage of the data lies within n standard deviation from the mean. The accuracy value will then be selected by choosing the associated standard deviation, θ, value.

When considering any optimisation process, care must be taken to ensure that the uncertainty range lies within the target bound within an acceptable accuracy.

2.3.3 Intensity Optimisation

To optimise the system, we are interested in making our SOBP curve as close as possible to a piecewise constant function as shown in Figure 7.

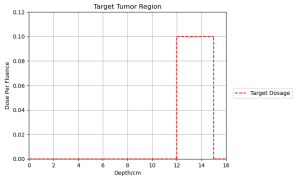

Figure 7: Target Tumor Doseage

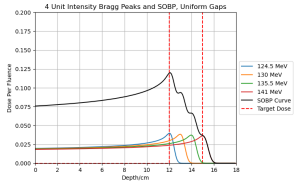

Figure 8: Uniformly Distributed Bragg Curves and SOBP Curve

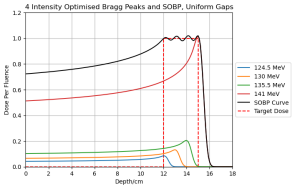

Figure 9: Intensity Optimised Bragg Curves and SOBP

Tackling this problem requires an introduction to terms listed in. We see that we would like to acquire some collection of n individual bragg peaks, b, with associated weights, ω, that cumulatively give us our optimised Spread Out Bragg Peak d.

Hence,

$$d = w_1 b_1 + ... + w_i b_i + ... + w_n b_n, \text{for } i \in [0,1,...,n] \tag{7}$$

Let Ω be our whole domain and T be a subset of Ω such that T is the 1D range of our tumor.

Furthermore, let,

$$\underline{\underline{A}}_{i,j} = \int_T b_i(x) b_j(x).dx \tag{8}$$

Now we wish to construct our solution vector, $\underline{f}$, with our previously stated dose piecewise constant dose function d_T, and non zero piecewise constant value, c.

Hence, let,

$$\underline{f}_i = \int_\Omega d_T b_i(x) = \int_T c b_i(x) \tag{9}$$

Solving the formulated linear system, $\underline{\underline{M}}\underline{\omega} = \underline{f}$ for ω, gives us the weights for our optimised SOBP solution. This optimisation process has been applied to Figure 9 and has proved suitable although not foolproof.

Care must be taken to provide the following variables:

- Initial energy, E_0, must be predefined for every Bragg curve in the collection of Bragg curves, $b_i \in b$.
- Displacement of peak, x_{peak}, should be less than the upper limit of the tumor range. An example of this can be seen in Figure 11, where the Bragg curve with the largest x_{peak} has been favoured due to the smoothness of the Bragg curve prior to the peak. This results in an impressive amount of over radiation outside of the tumor region.

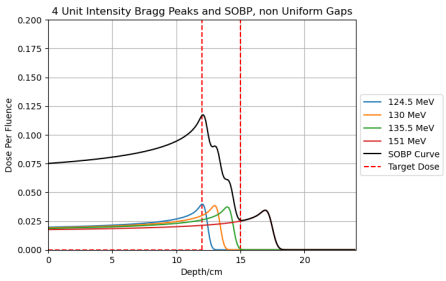

Figure 10: 4 Unit Intensity Bragg Peaks and SOBP, non Uniform Gaps

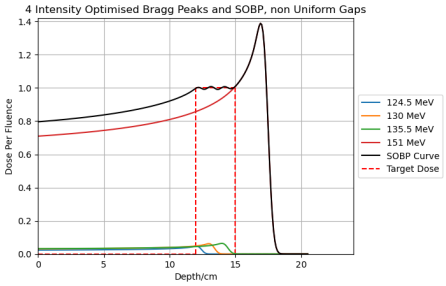

Figure 11: 4 Intensity Optimised Bragg Peaks and SOBP, non Uniform Gaps

After reviewing Figure 11, the logical step is to improve our optimisation process to include the minimisation of the difference between the SOBP curve and the Target dosage curve for the whole domain, instead of just the Target region. However, we should first define a way to display percentage error.

2.3.4 Error

Error, $\mathbb{E}$, over our target tumor region, T, in a continuous case takes the known form of,

$$\mathbb{E} = \sqrt{\int_T (d-c)^2.dx} \tag{10}$$

Figure 13 shows an example of the Error for some, n, uniformly spaced Bragg curves against n. We see that there exists some minimum Error at $n = 10$, and $\forall n > 10 : E_n > E_{10}$. This is thought to be caused by the Gibbs Phenomenon (Gottlieb & Shu, 1997) and hence there exists some minimum to the Error plot for which we take as the most optimal n for the uniform distribution model paired with the Bortfeld General Model. Taking the integral of such a function

defined in (1) require the use of quadrature methods (Ma, Rokhlin, & Wandzura, 1996) to approximate to a degree acceptable of our use.

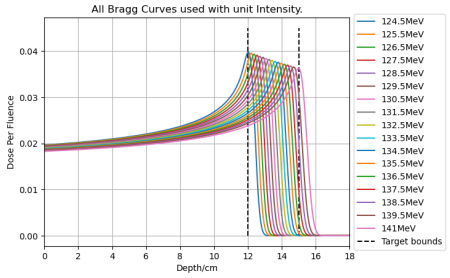

Figure 12: BGM: All Bragg Curves used during iterative uniform distribution process.

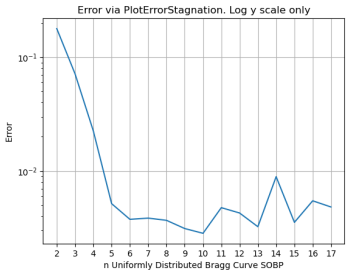

Figure 13: BGM: Error against n curves used to make SOBP

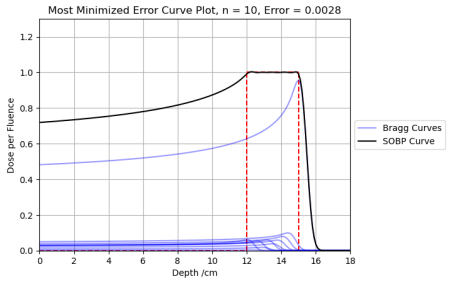

Figure 14: BGM: Least Error Intensity Optimised SOBP .

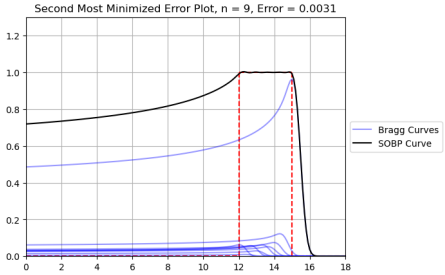

Figure 15: BGM: Second Least Error Intensity Optimised SOBP

2.3.5 Shallow Tumor Example

As mentioned before and observed in Figure 3, we can see that for larger initial energy values, or equivalently, larger x_{peak} values, we see that a Bragg curve has smaller D_{peak} and also the gradient around x_{peak} becomes smoother.

Intuitively, it is obvious that the maximum value of the second derivative decreases after reviewing Figure 2 but made clear after reviewing Figure 16. Care was taken to ensure the optimisation could sufficiently provide an Intensity Optimised SOBP with acceptably low error under the conditions of shallower depth tumors, and hence, less smooth Bragg curves. We see that the least Error SOBP for a shallow tumor range, unsurprisingly has more individual Bragg peaks than in a deeper tumor example in Figure 20. This example still suffers from the Gibbs Phenomenon due to there being a critical point where Error has a minimum at $n = 23$, and $\forall n \neq 23 : E_n > E_{23}$.

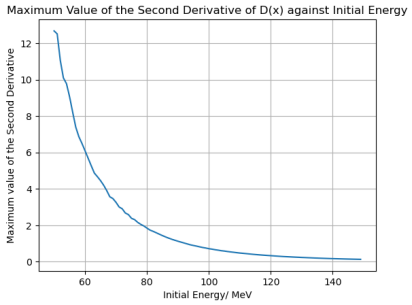

Figure 16: Maximum Value of Second Derivative against Initial Energy

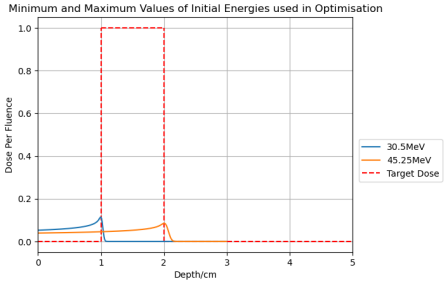

Figure 17: BGM: Shallow Target Tumor Region

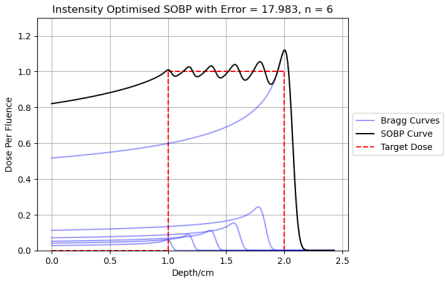

Figure 18: BGM: n = 6 case Intensity Optimised

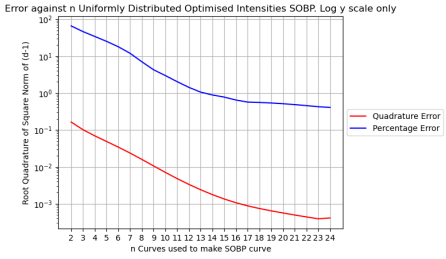

Figure 19: BGM: Calculated Error (10) and Percentage Error for each Intensity Optimised SOBP,

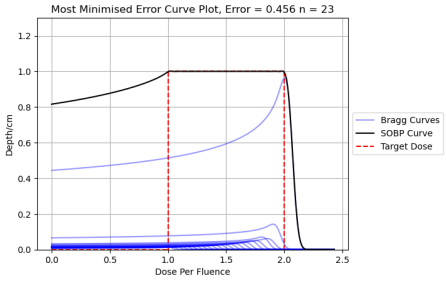

Figure 20: BGM: Least Error Plot, n = 23

2.3.6 Further Intensity Optimisation

Now we have defined the suitable way to calculate Error in SOBP over some tumor range, we can proceed in improving the optimisation process by altering what $\underline{\underline{A}}$ is defined as. We do this by appending a term which takes into account the area outside the tumor range to be minimised to the dose piecewise constant function that resides at 0 for all values outside the target tumor range, seen as

(11).

$$\underline{\underline{A}}_{i,j} = \theta \int_T b_i(x)b_j(x).dx + \sigma \int_{\Omega/T} b_i(x)b_j(x).dx \tag{11}$$

The use of θ and σ have been implemented to allow for a ratio of the optimisation to account for optimising over the tumor range to the whole domain. Using the model containing σ and θ, we can deduce that for all $\sigma > 0$, the Error calculated via (10) shall give a worse Error value than using a model with (11).

Another step to improve the optimisation is to penalise the derivative of the SOBP, d, to hence select the smoothest curve in hope to reduce the distortion caused by the Gibbs phenomenon as can be seen in Figure 13, $\forall n > 10$. We do this by following a Tikhonov regularisation (Golub, Hansen, & O'Leary, 1999) to produce the new equation of $\underline{\underline{A}}$ in (12), which is now a non-linear system.

$$\underline{\underline{\hat{N}_{ij}}} = \theta \int_T b_i(x)b_j(x).dx + \sigma \int_\tau b_i(x)b_j(x).dx + \psi \int_T |\hat{d}'(x)|^{p_{2_0}-2} b_i'(x)b_j'(x).dx \tag{12}$$

Where $\hat{d}(x) = \sum \hat{\omega}_i b_i(x)$ Solves $\hat{N}\omega = \underline{f}$ for $p_{2_1} > p_{2_0}$. Furthermore where, p_2 is a Sobolev conjugate (Arriagada, 2021), (13).

$$\frac{1}{p} + \frac{1}{q} = 1 \tag{13}$$

Solving this system results in optimal models however once compared to the model using (11), proves to give worse Error results, for any value of p_2 - as can be seen from [insert references here].

Due to the optimisation process of (11) where $\sigma = 0$, or equivalently, the optimisation process of (8) resulting in the least Error value, $\mathbb{E}$, we shall take this as the general optimisation model for all cases unless specified otherwise.

2.3.7 Conclusion of Bortfeld's General Model

Using the intensity optimisation method stated earlier, on the Bortfeld General Model has been able to achieve a SOBP, with weighted, uniformly distributed, Bragg curves that can give Error over our Target region of less than 1%. Example of this has been shown in Figures 14 and 20

3 Model 2. FLUKA Model

After suitable modelling had been applied to the Bortfeld's General Model, comparisons were made to FLUKA Monte Carlo (Parodi, Ferrari, Sommerer, & Paganetti, 2007) models of SOBP's. Examples of the Raw data calculated with the density of Lung, $\rho_L = 300kgm^{-3}$, can be seen in Figure 21, and examples of the differences can be seen in Figure 22.

Although the density of the mediums are different, Bortfeld's General Model dictates, (1), density is regarded to be a constant at the start of the equation,

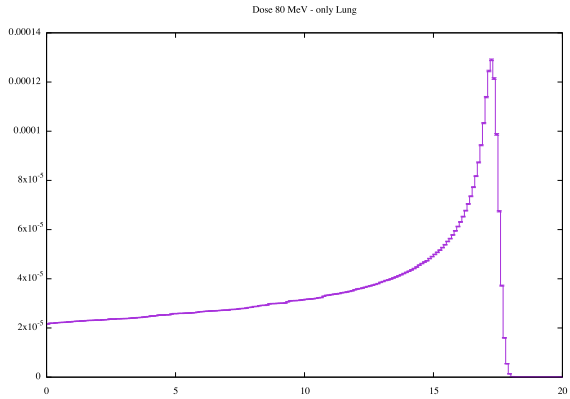

Figure 21: FLUKA model of 80 MeV Bragg curve through lung

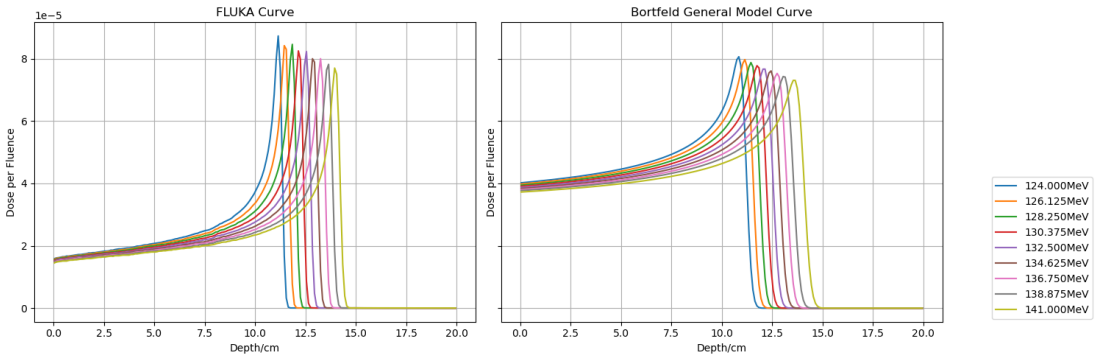

Figure 22: Comparison of Fluka Model to Bortfeld General Model

hence not affecting the difference of Dose per Fluence value of the tail prior to the peak, at the peak, and after the peak. This implies we need a new model to more accurately represent the FLUKA model in python if we wish to optimise this model with our already defined optimisation techniques. However, with enough data produced from the FLUKA model we can still apply our optimisation process to the curves. This time, instead of dealing with a continuous case that our previous Bortfeld General Model catered for due to having (1) to represent the curve. we now need a way of completing the same optimisation but for a discrete case, due to the resulting FLUKA model providing information in the form of a .csv file.

Hence, the new equation for $\underline{\underline{A}}$ is as follows,

$$\text{Let } f_{i,j}(x) = \begin{cases} b_i(x)b_j(x) & \forall x \in T \\ 0 & \forall x \notin T \end{cases} \tag{14}$$

$$\underline{\underline{A}}_{i,j} = \frac{1}{2}\sum_{k=1}^{n}(x_k - x_{k-1})[f_{i,j}(x_{k-1}) + f_{i,j}(x_k)] \tag{15}$$

Similarly, the new equation for $\underline{h}$ is,

$$\underline{h}_j = \frac{d_T}{2}\sum_{k=1}^{n}(x_k - x_{k-1})[b_j(x_{k-1}) + b_j(x_k)] \tag{16}$$

And finally, we may approximate the equation for the Error, $\mathbb{E}$ as:

$$\text{Let, } g(x) = (d(x) - c)^2 \tag{17}$$

$$\mathbb{E} \approx \sqrt{\frac{1}{2}\sum_{k=0}^{n}(x_k - x_{k-1})[g(x_{k-1}) + g(x_k)]}. \tag{18}$$

In Figure 23, we see the optimised FLUKA model after using the defined discrete equations for our model. It may be assumed that the FLUKA model shall follow the properties of Error stagnation of what we had seen in Bortfeld's General Model in Figure 14. However, due to the scarcity of data available during the research we are unable to conclude such a claim. Never the less, we may still compute Error via Equation (17), which has been included in the title of Figure 23.

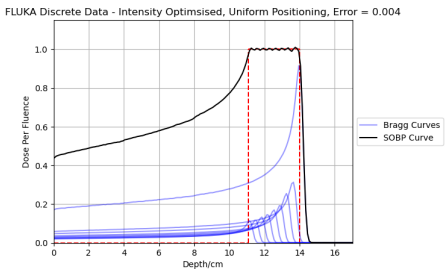

Figure 23: Python FLUKA Model of Optimal Intensities Applied from Optimisation.

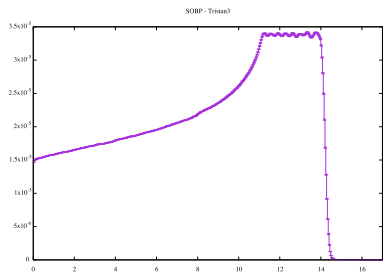

Figure 24: FLUKA Model of Optimal Intensities Applied from Optimisation.

4 Model 3. Bortfeld's H20 Model

In (Bortfeld, 1997), we also see a more H20 specific model, which had been compared to the FLUKA model in Figure 25.

$$D(x, E_0) = \Phi_0 \frac{e^{-(R_0-x)^2/(4\sigma^2)}\sigma^{0.565}}{1 + 0.012R_0} \times [11.26\sigma^{-1}\mathbb{D}^{-\zeta}_{-0.565} + (0.157 + 11.26\epsilon/R_0)\mathbb{D}^{-\zeta}_{-1.565}]. \tag{19}$$

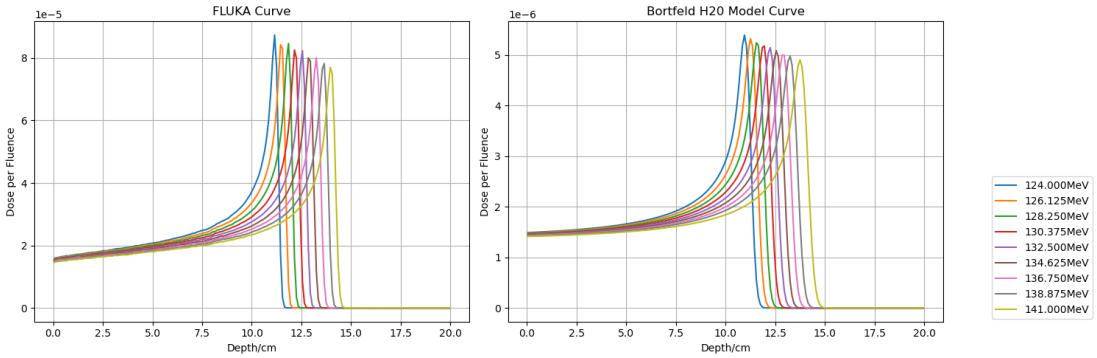

Figure 25: FLUKA and Bortfeld's H20 model comparison

Where Once again, $\mathbb{D}$ is the Parabolic Cylinder Function (Weisstein, 2002), Φ_0 is defined as in (2) and ζ is defined as in (3). Further details on the variables used in the model can be found in (Bortfeld, 1997), of which many depend on the Initial Energy, E_0.

This model seems to more accurately model the FLUKA curves than Bortfeld's General model, however differences still occur and inhibit using the H20 model as a direct model for FLUKA, a more close comparison of a single Bragg curve can be seen in Figure 26. An example of the H20 model used to optimise the system for the FLUKA model can be seen in Figure 28.

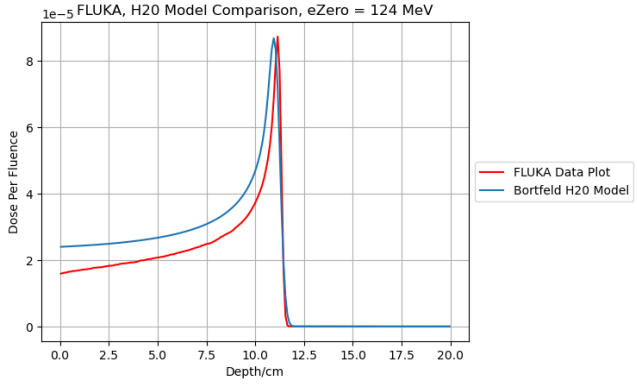

Figure 26: FLUKA, Bortfeld H20 comparison. $E_0 = 124MeV$

After reviewing the Figures above, it is clear to see that current models of FLUKA are inaccurate to a degree that renders the models unusable once compounding errors occur in the SOBP process. However, as stated before, working with discrete data from FLUKA models can be used to still give an optimised solution.

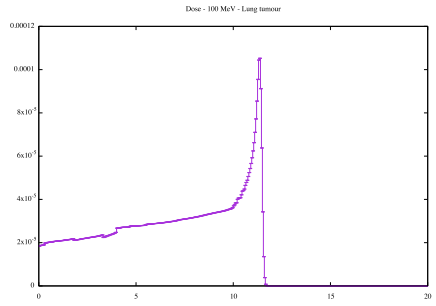

Figure 27: FLUKA model with multiple changing density mediums

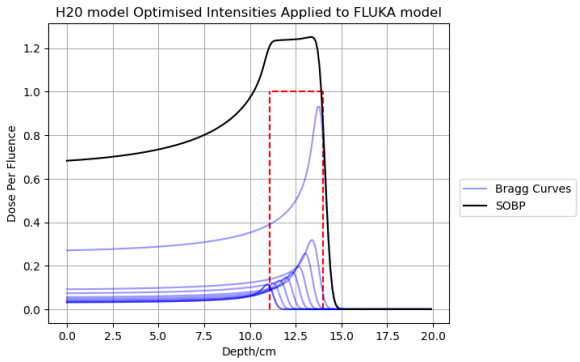

Figure 28: Bortfeld H20 model Optimised and Intensities Applied to FLUKA model

5 Model 4. Density Changing Model

Our prior models had not considered changing densities, this plays a significant role into our models due to the effect of dosage to medium density relationship changing per density.

In practice, tumors are located behind different mediums with different density profiles. This affects the amount of dosage deposited in each medium and hence produces a Bragg curve like the FLUKA model in Figure 27, where there are piecewise segments of the curve relative to the medium travelling through.

We therefore need a new model to keep track of how much Energy is remaining (yet to be transferred to the medium), and calculate Bragg curves through different densities.

The model is built using (1) due to all the variables listed below being included in the (1), unlike 19 which assumes the medium is water.

Many of the variables used in the prior models had also been predefined in relation to the density of water, hence for a changing density model we shall need to clarify a few terms that will be variables in our next model. In our next model it is essential that not only density, ρ, is changed but all the parameters listed below that we have seen before in (1).

- p. Defined as the "Exponent of Range-Energy relation", this unit less variable has been used to change the displacement of the peak.
- α. Defined as the "Proportionality Factor" (Bortfeld, 1997), with units of $cmMeV^{-p}$, has been used to change the displacement of the peak and maximum height of the peak.
- ρ. Density of the medium was taken to be $997kgm^{-3}$ and since will be variable. This has the affect of multiplying the curve by a constant.

- ϕ. A new variable, not to be confused with the ϕ in (12), which shall denote the displacement at which a density may change. Should we expect a medium to exist for $2cm$ at depth $5cm$ and have medium of water at all displacement othereise, we may say: $_1 = 5, \phi_2 = 7$.
- $\underline{x}$ and x_i. $\underline{\mathrm{x}}$ is the entire region for the model to be computed over defined in (28) and defined in (22). Whereas x_i is a subset as defined in (20).
- $E(x)$. Defined in (21). This is the amount of Energy left to be deposited to the medium by the Bragg Curve at depth x.

$$x_i \subset \underline{x} \tag{20}$$

$$E(x) = \frac{1}{\alpha^{1/p}}(R_0 - x)^{1/p} = \frac{(R_0 - x)^{-p}}{\alpha} \tag{21}$$

$$\underline{x} = x_1 \cup x_2 \cup ... \cup x_n \text{ for } i \in \text{ [1, 2,..., n]} \tag{22}$$

First we need a way to see how much Energy a Bragg curve has at certain depth (21), with a graphical interpretation in Figure 30.

Let,

$$\begin{gathered} E_1(x) = E(x, \rho_1) \\ E_2(x) = E(x, \rho_2) \\ E_3(x) = E(x, \rho_3) \\ \text{where, } \rho_1 \neq \rho_2 \neq \rho_3 \end{gathered} \tag{23}$$

define Three equations for (21) for some non equal arguments. We seek to find some

$$\begin{gathered} \hat{x}_1 : E_1(x) = E_2(x) \\ \text{and,} \\ \hat{x}_2 : E_2(x) = E_3(x) \end{gathered} \tag{24}$$

Such that,

$$E^s(x) = \begin{cases} E_1(x) \ x \leq \hat{x}_1 \\ E_2(x - \hat{x}_1) \ x_1 \leq x \leq x_2 \\ E_3(x - \hat{x}_2) \ x \geq x_2 \end{cases} \tag{25}$$

.

Similarly, for a general case,

$$E^s(x) = \begin{cases} E_1(x) \ x \leq \hat{x}_1 \\ ... \\ E_i(x - \hat{x}_{i-1}) \ x_{i-1} \leq x \leq x_i \\ ... \\ E_n(x - \hat{x}_{n-1}) \ x \geq x_n \end{cases} \tag{26}$$

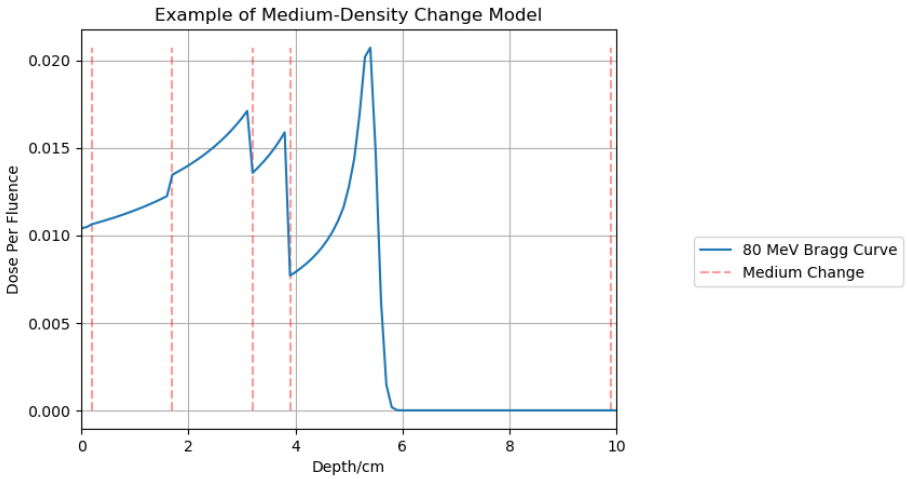

Figure 29: Example of Medium - Density Change Model

For $i \in (1, n)$.

Once constructed, we seek to find our equivalent Bragg peak representation,

$$\hat{D}^s(\underline{x}) = \begin{cases} D_1(x, p, \alpha, \rho) \ x \leq \hat{x}_1 \\ ... \\ D_i(x - \hat{x}_{i-1}) \ x_{i-1} \leq x \leq x_i \\ ... \\ D_n(x - \hat{x}_{n-1}) \ x \geq x_n \end{cases} \tag{27}$$

For $i \in (1, n)$.

What we see in (27) gives us what we observe in Figure 29, for some chosen, p, α, ρ, $\phi_{1,...,n}$.

Hence, let our new density changing model be defined with variables defined similarly to (1) aside from variable arguments, x_i, p, α, ρ, which are to be altered based on the medium of the density:

$$\hat{D}(x_i, p, \alpha, \rho) = \Phi_0 \frac{e^{-\zeta^2/4}\sigma^{1/p}\Gamma(1/p)}{\sqrt{2\pi}\varrho p\alpha^{1/p}(1 + \beta R_0)}[\frac{1}{\sigma}\mathbb{D}_{-1/p}^{-\zeta} + (\frac{\beta}{p} + \frac{\gamma}{\beta} + \frac{\epsilon}{/}R_0\mathbb{D}_{-1/p-1}(-\zeta))] \tag{28}$$

Intuitively, this leaves us with,

$$D(\underline{x}) = \hat{D}(x_1) \cup \hat{D}(x_2) \cup ... \cup \hat{D}(x_n) \tag{29}$$

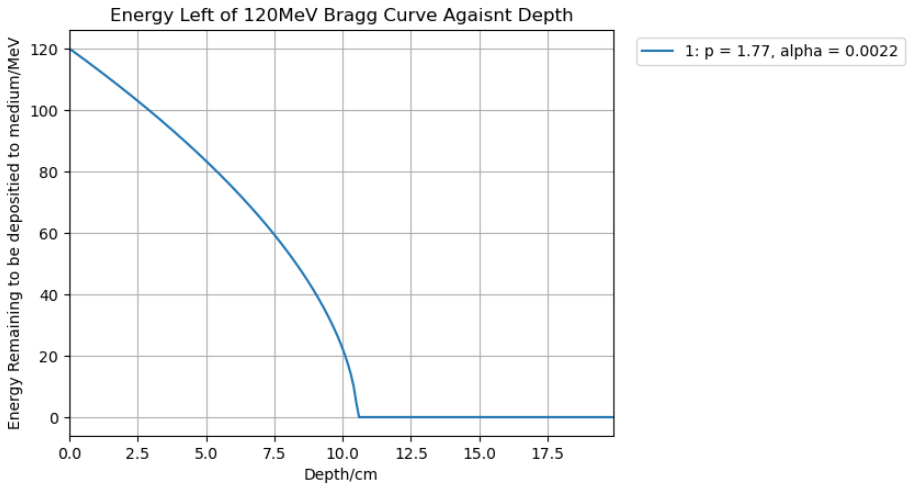

Figure 30: Energy Remaining to be deposited to medium against Depth of 120 MeV Bragg Curve

5.0.1 Optimisation of Density Model Intensities

Once again, we can use our optimisation method to calculate the correct intensities of the weights for a SOBP to reach a desired target tumor dosage. This time of a simplified changing density medium model as can be seen in Figure 33 and Figure 34.

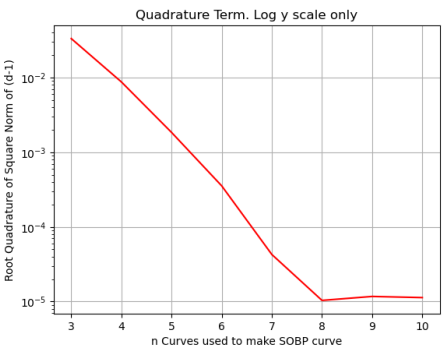

Figure 31: Quadrature Error (10) For Changing Medium Density Model

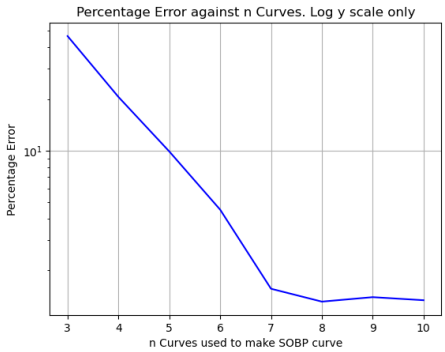

Figure 32: Percentage Error for Changing Medium Density Model

Once again, we see a minimum error at minimum Error at $n = 10$, and $\forall n > 10 : E_n > E_{10}$. This once again points towards the Gibbs phenomenon.

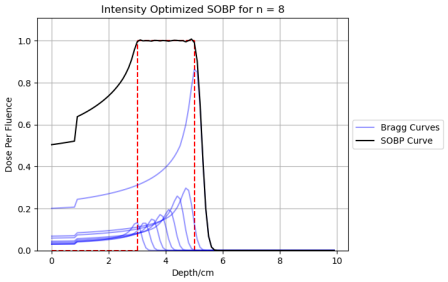

Figure 33: Least Error, Intensity Optimised SOBP, n = 8, Uniformly Distributed Bragg Peaks

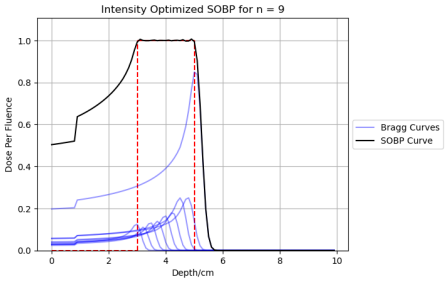

Figure 34: Second Least Error, Intensity Optimised SOBP, n = 9, Uniformly Distributed Bragg Peaks

References

Arriagada, W. (2021). Matuszewska–orlicz indices of the sobolev conjugate young function. *Partial Differential Equations in Applied Mathematics*, *3*, 100029.

Bortfeld, T. (1997). An analytical approximation of the bragg curve for therapeutic proton beams. *Medical physics*, *24*(12), 2024–2033.

Golub, G. H., Hansen, P. C., & O'Leary, D. P. (1999). Tikhonov regularization and total least squares. *SIAM journal on matrix analysis and applications*, *21*(1), 185–194.

Gottlieb, D., & Shu, C.-W. (1997). On the gibbs phenomenon and its resolution. *SIAM review*, *39*(4), 644–668.

Ma, J., Rokhlin, V., & Wandzura, S. (1996). Generalized gaussian quadrature rules for systems of arbitrary functions. *SIAM Journal on Numerical Analysis*, *33*(3), 971–996.

Parodi, K., Ferrari, A., Sommerer, F., & Paganetti, H. (2007). Clinical ct-based calculations of dose and positron emitter distributions in proton therapy using the fluka monte carlo code. *Physics in Medicine & Biology*, *52*(12), 3369.

Weisstein, E. W. (2002). Parabolic cylinder function. *https://mathworld. wolfram. com/*.